NANO: Brief Reports and Reviews Vol. 14, No. 5 (2019) 1950054 (10 pages) © World Scientific Publishing Company

DOI: 10.1142/S1793292019500541



# Femtosecond Laser-Assisted Synthesis of ZnO Nanoparticles in Solvent with Visible Emission for Temperature Sensing

Huanhuan Xu, Lihe Yan\*, Jinhai Si, Yanmin Xu and Xun Hou

Key Laboratory for Physical Electronics and

Devices of the Ministry of Education &

Shaanxi Key Lab of Information Photonic Technique

School of Electronics & Information Engineering

Xi'an Jiaotong University, Xi'an 710049, P. R. China

\*liheyan@mail.xjtu.edu.cn

Received 4 December 2018 Accepted 2 April 2019 Published 15 May 2019

Zinc oxide (ZnO) nanoparticles (NPs) are synthesized by one-step femtosecond laser ablation of zinc powders in n-methyl pyrrolidone (NMP) at room temperature. The as-prepared ZnO NPs are fairly stable, water-soluble and have abundant surface functional groups resulting in a strong fluorescence in the visible region. By further annealing the ZnO NPs in the reacting solvent up to 120°C, the photoluminescence (PL) intensity of material can be significantly enhanced. Besides, the PL of ZnO NPs can change from blue to green by controlling the annealing temperature. The products exhibit excellent temperature sensing with high temperature sensitivity and a 1.3% change per °C response over a linear temperature sensing range (6–84°C) in aqueous buffer, which matches well with the physiologically relevant temperatures. Hence, the ZnO nanoparticle system can serve as a promising candidate for practical fluorescent temperatures nanosensors which can be used for accurate temperature monitoring within biological systems.

Keywords: ZnO nanoparticles; temperature sensing; femtosecond pulsed laser ablation.

### 1. Introduction

Temperature sensing plays an important role in many areas such as micro/nano electronics, integrated photonic devices and especially in biosensing systems.<sup>1</sup> As conventional methods for measurement of temperature cannot be used in cells and other nanostructures, the use of molecular or nanoparticles (NPs)-based optical probes is the only way for intracellular temperature sensing.<sup>2</sup>

Fluorescent temperature sensors based on luminescent nanomaterials have attracted great attention due to their advantages of miniaturization, noncontacting features and high accuracy.<sup>3</sup> Luminescent semiconductor NPs with narrow size distribution and high luminescent efficiency have received intensive attention during the past decade, owing to their unique optical and electronic properties and promising applications ranging from displays to therapeutic agents and vivo biological

<sup>\*</sup>Corresponding author.

imaging.<sup>4–8</sup> However, the traditional quantum dots (QDs) based on CdTe and CdSe materials are harmful to the biological systems and human health.<sup>9</sup> Although various protections such as polymers and other nontoxic shells have been made to reduce the damage to the environment, the radicals derived from light irradiation and the decomposition of NPs by oxygen still might influence the biological systems.<sup>10–12</sup> Hence, environmentally friendly luminescent semiconductors NPs would be desirable.

ZnO has attracted attention for optics and optoelectronics applications, due to its unique attributes of good environmental stability, wide bandgap, good bio-compatibility, nontoxicity and low cost compared with traditionally used QDs of CdTe or CdSe. 13-16 Recently, research interests in ZnO QDs have developed to a much wider scope, from doping and surface modifications to altering optoelectronic properties. 17-19 Nevertheless, crystalline, chemically pure, nanosized-ZnO is still a challenge to synthesize for ZnO QDs.<sup>20</sup> As far as ZnO QDs are concerned, the sol-gel route has been the most effective approach to synthesize ZnO QDs dispersions.<sup>21</sup> Unfortunately, colloidal ZnO nanocrystals synthesized by the sol-gel route tend to aggregate due to their high surface energy.<sup>22</sup> Moreover, such surface modified ZnO colloids are usually well dispersed in organic solvents instead of water, limiting their use for bioanalysis.

Fabrication of nanostructures by pulsed laser ablation (PLA) in liquid phase has attracted much attention recently. 23-27 There have been recent reports on the synthesis of ZnO NPs using PLA method from Zn target in an aqueous solution containing different surfactants.<sup>28,29</sup> Due to its unique properties of ultra-short pulse duration and ultra-high peak power, femtosecond laser can supply an efficient alternative to prepare ZnO NPs by ablating the reactant zinc powder in solutions. In the synthesis process, the zinc powder and solution are ionized under the irradiation of pulsed laser and then a plasma with high temperature and pressure is formed.<sup>30</sup> With the expansion and collapse of the plasma plume, ZnO NPs are formed and connected to the functional groups on their surface simultaneously. 31 Though many synthesis strategies based on chemical methods have been explored to fabricate ZnO NPs, the involvements of environmentally hazardous chemicals and complex chemical processes largely restrict both the flexibilities of the

NPs. PAL method can provide a green one-step synthesis strategy of NPs. Generally, the size of the NPs prepared using PAL methods are only several nanometers, and the PL property of the NPs can be well controlled by adjusting the ablation parameters. Besides that, abundant functional groups can be attached on the surface of the NPs during the ablation process. Benefiting from these advantages, the NPs prepared using PAL have excellent water solubility and the suitability for subsequent functionalization with appropriate receptor molecules to be used for the imaging of cancer cells and bacteria.<sup>32</sup>

In this study, we present a one-step green route to synthesize water stable ZnO NPs with visible emission by femtosecond pulsed laser ablation in liquid at room temperature. The synthesized ZnO NPs are water-soluble, fairly stable and have a strong fluorescence in the visible region. From the TEM picture, the as-prepared ZnO NPs are monodisperse nanocrystals of near spherical morphology, and no large aggregations are observed. In addition, we can control the fluorescence properties of ZnO NPs by further annealing. Structural characterizations and spectroscopic analyses verify that abundant functional groups are created on the surface of the ZnO NPs, which are responsible for the visible emission of the ZnO NPs. Moreover, the as-prepared ZnO NPs demonstrate high temperature sensitivity over wide-ranging temperature, which can offer a beneficial temperature sensing platform of cellular environments.

#### 2. Experimental

#### 2.1. Chemicals

N-Methyl pyrrolidone (NMP) and zinc powders were purchased from Sinopharm Chemical Reagent Co., Ltd. Cellulose ester Dialysis membranes (membrane molecular weight cutoff  $\sim 1000$ ) used for dialysis were purchased from Aladdin Chemistry Co., Ltd (China).

# 2.2. Synthesis of ZnO NPs

The ZnO NPs were synthesized by femtosecond laser ablation of zinc powder in NMP at room temperature. In a typical procedure, 0.1 mg of zinc powder with a mean size of 600 nm was mixed with 50 ml of NMP liquid then ultrasonicated to obtain a uniform dispersion. A Ti: sapphire femtosecond

laser system with repetition rate of 1 kHz, pulse duration of 150 fs, central wavelength of 800 nm was used for laser ablation. 10 ml of dispersion is obtained by pipette and then put into a glass beaker for laser ablation. The laser power was 400 mW and the laser beam was focused into the dispersion by a 100 mm lens for 1 h. In order to prevent the suspended powders from gravitational settling in the solvent, a magnetic stirrer was used during the laser ablation. After laser ablation, large zinc particles were removed by centrifuging the dispersion at 2000 rpm for 20 min. Then the solution was annealed at different temperatures varied from 60°C to 120°C for 24 h. The obtained solution containing ZnO NPs was dialyzed against deionized water in a dialysis bag for 24 h to remove some impurities.

#### 2.3. Instrumentation

X-ray diffraction (XRD) of the ZnO NPs was carried out in a Bruker D8 ADVANCE. Samples were prepared by dropping suspensions of the ZnO NPs in water onto a glass substrate, followed by solvent evaporation in a dust protected atmosphere. Transmission electron microscopy (TEM) and high-resolution transmission electron microscopy (HRTEM) images were carried out on a

JEM-ARM200F microscope. Samples were prepared by dropping suspensions of the ZnO NPs in water onto Cu TEM grids coated with a holey amorphous carbon film, followed by solvent evaporation in a dust protected atmosphere. The measurements of fluorescence spectra were recorded on a FLS920 spectrometer (Edinburgh). UV-2600 spectrophotometer (Shimadzu) was employed to record the UV-Vis absorption spectra. X-ray photoelectron spectroscopy (XPS) data was measured by an AXIS ULtrabld XPS system. Samples were prepared by dropping suspensions of the ZnO NPs in ethanol onto a Silicon substrate, followed by solvent evaporation in a dust protected atmosphere. The Fourier transform infrared spectroscopy (FT-IR) was performed on VERTEX 70 (Bruker). Samples were prepared by dropping suspensions of the ZnO NPs in ethanol onto highly pure potassium bromide tableting, followed by solvent evaporation in a dust protected atmosphere.

#### 3. Results and Discussion

# 3.1. Characterizations of ZnO NPs

Firstly, the crystal structure and morphology of the as-prepared ZnO NPs is characterized by XRD and TEM images. As shown in Fig. 1(a), seven sets of

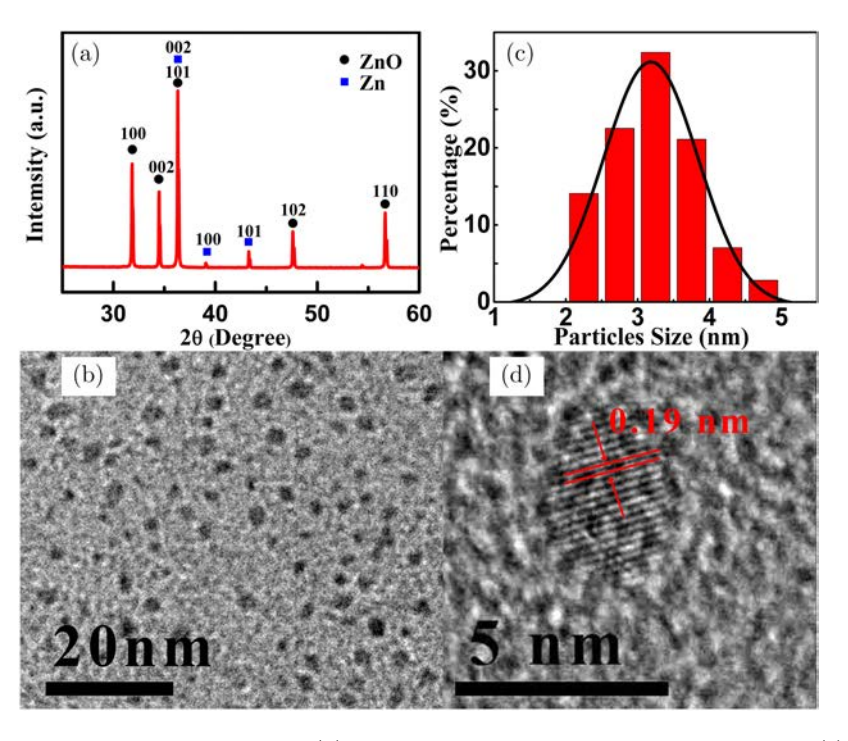


Fig. 1. (a) XRD patterns of as-prepared ZnO NPs, (b) TEM images of the as prepared ZnO NPs, (c) the corresponding size distributions of the ZnO NPs and (d) the HRTEM images of the ZnO NPs.

diffraction peaks can be observed, belonging to metal Zn and wurtzite ZnO crystals. As previously reported, 21,29,33 the appearance of five diffraction peaks corresponding to (100), (002), (101), (102), (110) fit well with ZnO with wurtzite structure (JCPDS Card No. 89-1397), while the other diffraction peaks are consistent with metal Zn which were not oxidized to produce ZnO NPs. We performed a semi-quantitative analysis of the asprepared samples, and the proportion of ZnO NPs was 97%. In the femtosecond laser ablation process, Zn plasma plumes with high temperature and high pressure are formed and the solvent is ionized simultaneously. When the plasma plume expands and cools down, Zn could be oxidized and aggregate into ZnO NPs with several nanometers size. In this process, a small amount of Zn atoms could be enclosed inside the ZnO NPs, and further oxidization is blocked, causing the inclusion of Zn elements in the ZnO NPs.

As shown by the TEM image in Fig. 1(b), the asprepared ZnO NPs are monodisperse nanocrystals of near spherical morphology, and no large aggregations are observed, meaning that the ZnO NPs are well dispersed in the water. Figure 1(c) shows the

size distributions of the ZnO NPs, the as-prepared ZnO NPs are in a narrow range of about 2–4.8 nm with the mean size of about 3.2 nm, which is smaller than that reported for ZnO NPs. 33–35 The HRTEM image is given in Fig. 1(d). From the figure, we can see that the lattice spacing distance of ZnO NPs is 0.19 nm, which was in close match with the (102) lattice spacing of ZnO (JCPDS Card No. 89-1397). XRD and TEM jointly show that the zinc powder has been transformed into ZnO NPs after liquid phase ablation by femtosecond laser.

More information about element analysis of the ZnO NPs is characterized by XPS given in Fig. 2. As shown in Fig. 2(a), besides the signals of C1s, O1s and N1s visible at 284.9 eV, 399.7 eV and 531.1 eV, the signal of Zn2p can be recognized at 1021.5 eV. The detailed C1s spectrum [Fig. 2(b)] shows three peaks with binding energies at 284.2 eV, 285.1 eV and 287.6 eV, corresponding to C–C, C–O and C=O, respectively.<sup>31</sup> Figure 2(c) shows the partial XPS spectrum of N1s, by peak fitting N1s can be resolved into two components centered at 399.3 eV and 399.6 eV, which confirms the formation of N surfaced doped ZnO NPs. In the deconvoluted Zn2p spectrum [Fig. 2(d)], two peaks at 1020.6 eV and

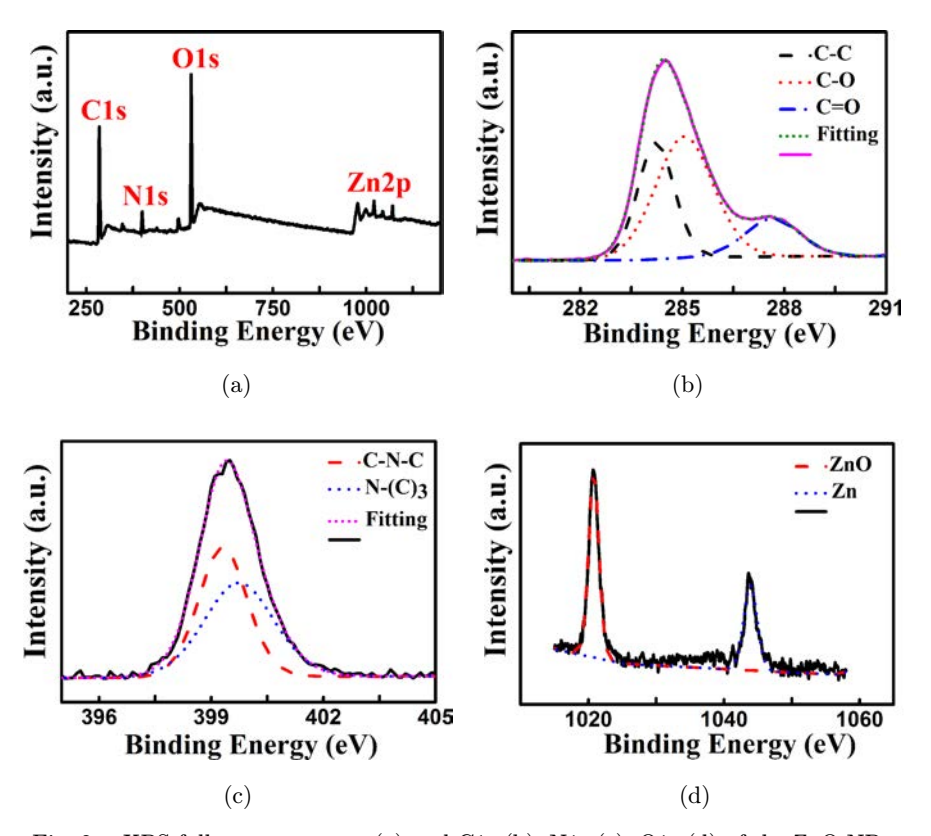


Fig. 2. XPS full scan spectrum (a) and C1s (b), N1s (c), O1s (d) of the ZnO NPs.

1043.8 eV reveal the presence of ZnO NPs.<sup>36</sup> The XPS spectrum suggests that ZnO NPs surface contains a large number of functional groups which could make the ZnO NPs stable in aqueous solution.

# 3.2. Optical properties of the ZnO NPs

# 3.2.1. Room temperature photoluminescence study

The UV-Vis and PL spectra of the as-prepared ZnO NPs are given in Fig. 3 to explore their optical properties. In the UV-Vis spectrum [Fig. 3(a)], there are two small optical absorption peaks at 285 nm and 356 nm. The peak at 285 nm is typically ascribed to  $n \to \pi^*$  of C=O, while another around 356 nm can be related to electron transition of  $n \to \pi^*$  for C=N, which are contained in the functional groups on the surface of ZnO NPs.<sup>37</sup> In the fluorescence spectra [Fig. 3(b)], the ZnO NPs show strong fluorescence emissions by excitation from 300 nm to 480 nm. The strongest fluorescence emission centered at around 435 nm is observed when excited by 360 nm excitation. Furthermore, excitation-dependent PL behaviors were observed when the excitation wavelength ranged from 300 to 480 nm, which could be attributed to the different functional groups on the surface of the ZnO NPs. Compared with other previously reported ZnO NPs, ZnO NPs prepared in this work have the advantages of the different visible light emission with different wavelength excitation.<sup>29,33,38</sup>

# 3.2.2. Effect of annealing temperature on ZnO NPs emission

In order to obtain highly fluorescent ZnO NPs with a broad fluorescence emission, ZnO NPs were annealed for 24 h in NMP solvent from 60–120°C. Figures 4(a)-4(d) show the PL spectra of the ZnO NPs annealed with different temperature of (a) 60°C, (b) 80°C, (c) 100°C and (d) 120°C, respectively. To avoid the change of the physical properties of solvents by heating, the highest annealing temperature (120°C) was kept lower than the boiling point of NMP (203°C). The emission of the ZnO NPs after annealing is similar to the samples without annealing, which have an excitation-dependent PL behavior. The difference is that the maximum excitation wavelength changes with increasing annealing temperature. Although the maximum excitation wavelength of the ZnO NPs annealed at 60°C is the same as the unannealed samples, the PL intensity has an obvious increase when excited above 360 nm. When annealed at 80°C, the maximum excitation and emission wavelengths of the ZnO NPs are 380 nm and 452 nm. As the annealing temperature increases from 100°C to 120°C, the maximum excitation and emission wavelengths of the ZnO NPs also changed from 400 nm and 479 nm to 420 nm and 508 nm. As can be seen in Fig. 4, the maximum excitation and emission wavelengths and PL intensity of the ZnO NPs show a red-shift as a result of annealing. By controlling the annealing temperature, the PL of ZnO NPs can change from blue to green, which can be applied to multi-color imaging applications.

Here, we give a brief interpretation about the effects of thermal annealing on the PL spectra of ZnO NPs. In the PL spectra of ZnO, typically there are emission bands in the ultraviolet (UV) and visible regions. Even though the UV emission is usually attributed to the interband transition or the exciton combination in ZnO, the emissions in the visible region are still quite controversial among

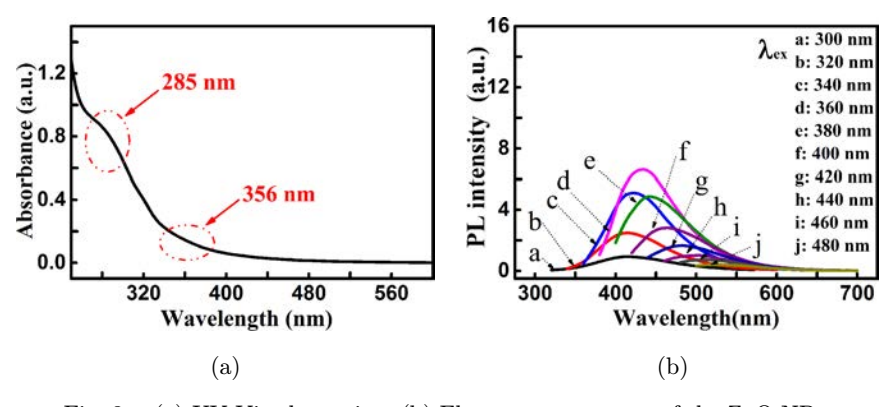


Fig. 3. (a) UV-Vis absorption, (b) Fluorescence spectra of the ZnO NPs.

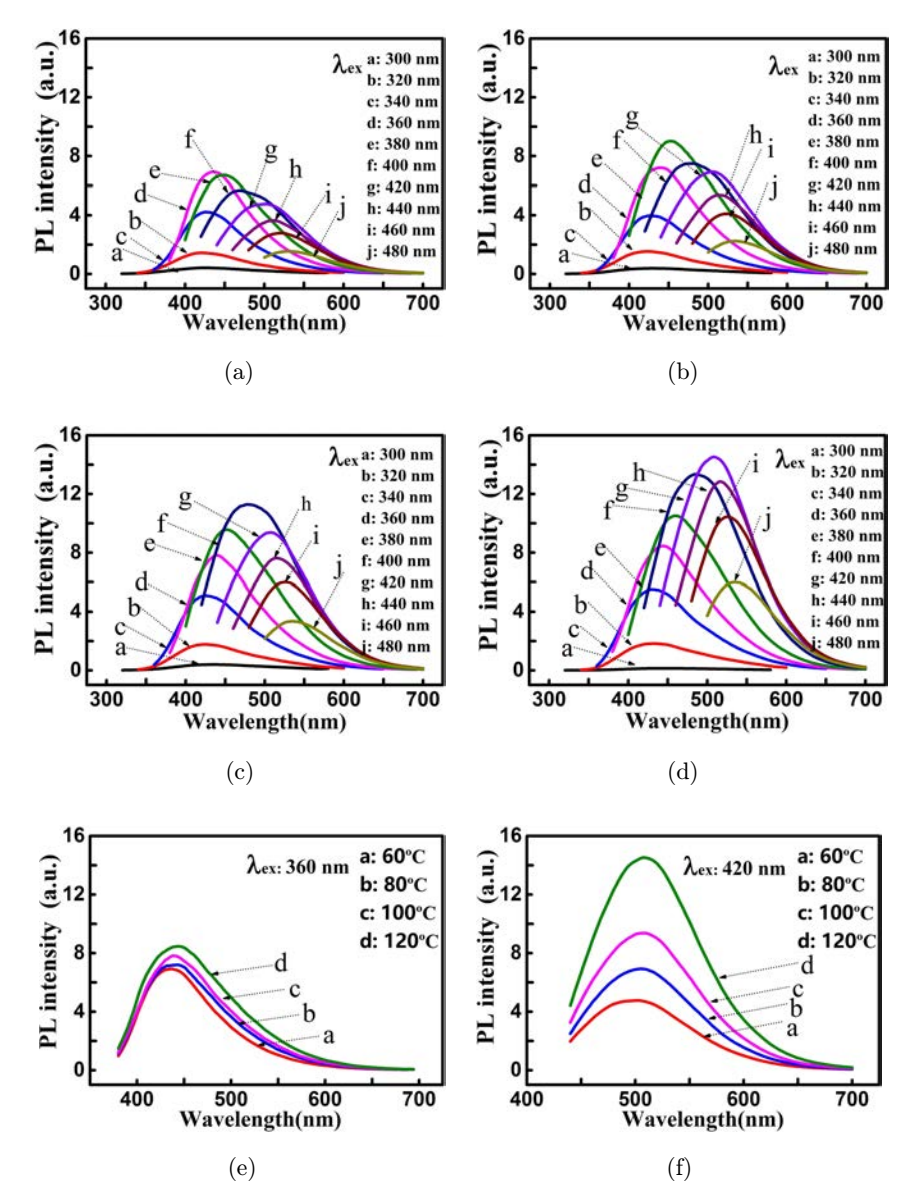


Fig. 4. Fluorescence spectra of ZnO NPs annealed with different temperature of (a)  $60^{\circ}$ C, (b)  $80^{\circ}$ C, (c)  $100^{\circ}$ C and (d)  $120^{\circ}$ C and Fluorescence spectra of the ZnO NPs at different excitation wavelength of (e)  $360 \,\mathrm{nm}$ , (f)  $420 \,\mathrm{nm}$ .

researchers.<sup>39,40</sup> Since the fluorescence emission peak of ZnO NPs synthesized by femtosecond laser ablation method is distributed in the visible regions, which is similar to that of carbon nanodots synthesized by femtosecond laser ablation method, we think that the surface functional groups of ZnO NPs play a key role in the effect of its PL.<sup>31</sup> In this study, further chemical reactions between the ZnO NPs and the solution molecules would take place in the annealing process, and more functional groups would be attached on the surface of the NPs, enhancing their fluorescence. With the increase of annealing temperature, the amount of the functional groups would be increased and the fluorescence is

further enhanced. Besides that, some carbon–nitrogen bonds might be broken from NMP at high temperature. These bonds connected on the NPs will cause the red-shift of the fluorescence emission. Figures 4(e) and 4(f) show the PL spectra of the ZnO NPs annealed at different temperature when excited at 360 nm and 420 nm, respectively. As shown by the figure, the PL intensity increases a little when excited at 360 nm, while it increases a lot when excited at 420 nm. This is because higher temperatures result in more nitrogen-containing functional groups than oxygen-containing functional groups attached to the ZnO NPs surface. Therefore, the maximum excitation and emission wavelengths and PL intensity of

the ZnO NPs show a red-shift as the annealing temperature increases.

FT-IR are performed to further demonstrate our prediction about effect of annealing process on the functional groups of the as-prepared ZnO NPs. The FT-IR spectrum of the ZnO NPs is given in Fig. 5. It can be seen from the figure that the absorption bands at around 1100 cm<sup>-1</sup> are attributed to the stretching vibrations of C-O. There are also stretching vibrations of C=C and C=O at around  $1560\,\mathrm{cm^{-1}}$  and  $1650\,\mathrm{cm^{-1}}$ . In addition, the absorption bands at around  $2920\,\mathrm{cm}^{-1}$ ,  $2850\,\mathrm{cm}^{-1}$  and  $1415\,\mathrm{cm^{-1}}$  correspond to the stretching and bending vibrations of  $\mathrm{CH}_2$  and  $\mathrm{CH}_3$ .<sup>31</sup> Besides, the absorption bands at around  $3360\,\mathrm{cm^{-1}}$  are attributed to the stretching vibrations of N-H, indicating that N atoms were effectively doped on the surface of the ZnO NPs. However, the peak location of NH<sub>2</sub> shows blue shift as the temperature increases. Previous studies have proved that the positions of the peaks produced by different kinds of amides and symmetric or nonasymmetric stretching vibrations are slightly different. Therefore, we think that the different annealing temperatures may lead to different kinds of amides and have a certain impact on the symmetry of the NH<sub>2</sub> stretching vibration.<sup>41</sup> Compared to the ZnO NPs without annealing, the annealed ZnO NPs at different temperatures obviously contain more functional groups on their surface. As the annealing temperature increases, the increment of nitrogen containing bonds is significantly higher than that of carbon-oxygen and the carbon-oxygen double bond. This is because the bond energy of the carbon-nitrogen bond is larger than the carbon-oxygen bond. 42 As the annealing temperature increases, the number of carbonnitrogen bonds broken from the NMP is larger than the carbon-oxygen bond, which will lead to more nitrogen functional groups on the surface of the ZnO NPs. The FT-IR results confirmed that the surface of the ZnO NPs is mainly covered with hydroxyl, carboxyl and nitrogen functional groups, which will have a significant effect on their fluorescence characteristics. To exclude the influence of the annealing process on the crystal structures of the formed ZnO NPs, XRD analysis of the NPs annealed with different temperature are further performed. As the annealing temperature increases, diffraction peak intensity of Zn changes very little, and the proportion of Zn was estimated 3\%, 5\%, 4\% and 5\% by semi-quantitative analysis, respectively. The small change in the content of Zn is thought to be due to the ablation process, while the annealing process influences only the surface functional groups on the NPs rather than the chemical structures of the ZnO NPs cores. Besides, the TEM image and the size

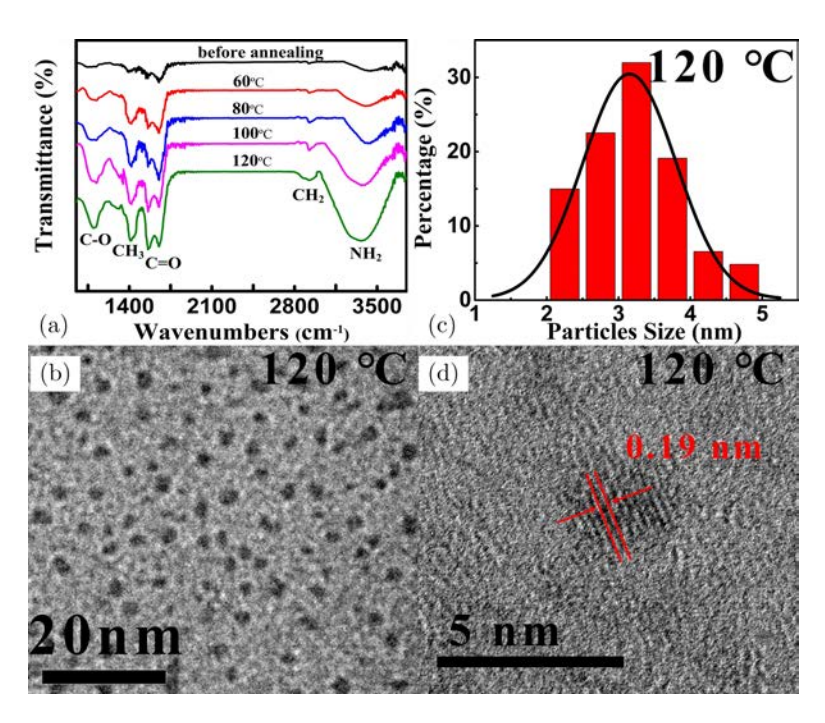


Fig. 5. (a) FT-IR spectra of ZnO NPs annealed with different temperature. (b) TEM images of the as prepared ZnO NPs, (c) the corresponding size distributions of the ZnO NPs and (d) the HRTEM images of the ZnO NPs annealed at  $120\,^{\circ}$ C.

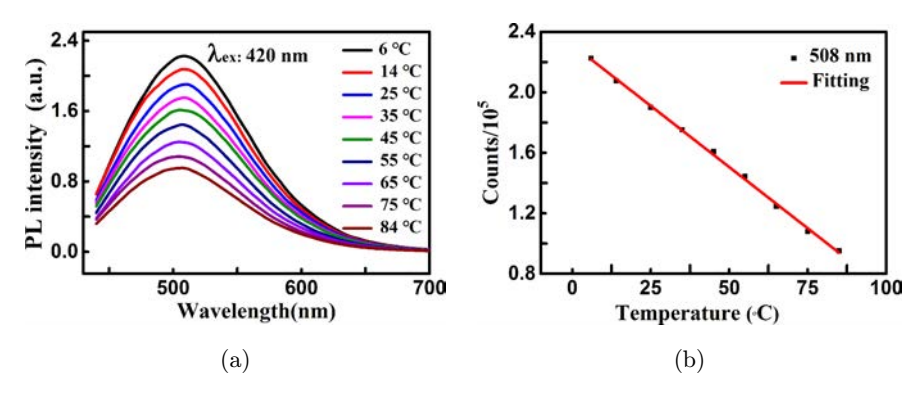


Fig. 6. (a) Fluorescence spectra of ZnO NPs at different temperatures excited at 420 nm, (b) The fluorescence intensities of the 508 nm peaks as a function of temperature were plotted for the ZnO NPs.

distributions of the ZnO NPs [Figs. 5(b)–5(d)] annealed at temperature of 120°C also show that the morphology of ZnO NPs is almost unchanged.

# 3.3. Temperature sensing

Since temperature influences is a fundamental thermodynamic parameter in cellular environments, affecting reaction kinetics and the physical states of nucleic acids and proteins, it is important to develop techniques and devices that are capable of accurately monitoring temperature within biological systems. 43-45 Although the traditional method based on thermocouple is sensitive and accurate, it cannot measure temperature remotely in narrow confined space or at many locations simultaneously. Owing to its noninvasive, which makes the approach suitable for biological imaging experiments, the nanoparticle-based temperature sensors have attracted increasing attention, recently. 46,47 Since our ZnO NPs have a strong fluorescence without conjugate with fluorescein isothiocvanate, it may have huge potential applications in biosensing. We next investigated the temperature sensitivity of ZnO NPs. Figure 6(a) show the fluorescence spectra of the ZnO NPs as a function of temperature when excited at 420 nm. As can be seen from the figure, the fluorescence intensities of 508 nm peaks gradually decrease with the increase of temperature due to the thermal activation of nonradiative-decay pathways. The temperature dependence of electronic states in semiconductors has been studied extensively, there are a huge number of researchers agree that the nonradiative relaxation is most likely the contributing factor due to the thermal activation of nonradiative trapping, which are often observed in semiconductor bulk, quantum dots, and core-shell

structured QDs. 48-50 At low temperatures, the nonradiative channels are not thermally activated; therefore, the excited electrons can radiatively emit photons. When the temperature rises, the nonradiative channels are thermally activated, such as trapping by surface/defect/ionized impurity states, resulting in a decrease in the quantum efficiency and fluorescence intensity.<sup>51</sup> To quantitatively determine whether the temperature-dependent changes in the emission spectra could be used for accurate temperature sensing, we plotted the change of the fluorescence intensity of the 508 nm peak [Fig. 6(b)]. The change of fluorescence intensity and temperature is linear in a wide temperature range from 6°C to 84°C (R2 = 0.998). Temperature-sensitive ZnO NPs showed a fluorescence intensities change of 1.3% per °C, which is comparable with that of other materials. 52-54 This indicates that the ZnO NPs can be used as a conventional intensity-based temperature sensor with high sensitivity. Besides, the sensing range (6–84°C) of ZnO NPs can covers both the physiological temperature for biology studies and the working temperature for many electronic devices. Thus, we believe ZnO NPs will become a useful tool for highly spatiotemporally resolved temperature measurements in many practical applications especially in cells and tissues.

#### 4. Conclusions

In conclusion, ultra-small ZnO NPs with excitation-dependent fluorescence are synthesized by using PAL method. As abundant functional groups are created on the surface, the prepared ZnO NPs exhibit excellent water solubility and bright PL emission in the visible range. By annealing the NPs at different temperatures, the fluorescence of the

NPs can be adjusted from blue to green. The ZnO NPs have a linear temperature sensing range (6–84°C) that matches well with the physiologically relevant temperatures and high sensitivity with 1.3% per °C, which make the ZnO NPs as promising candidate for temperature sensing. Hence, we believe that the as-prepared ZnO NPs can serve as a promising material to construct practical fluorescent temperature nanosensors which can be used for accurately monitoring temperature within biological systems.

### Acknowledgments

This work was supported by National R&D Program of China (2017YFA0207400), and the National Natural Science Foundation of China (Grant Nos. 61427816, 11674260 and 11474078), Key Research and Development Plan of Shaanxi Province with Grant no. 2017ZDXM-GY-120, the Fundamental Research Funds for the Central Universities, and the Collaborative Innovation Center of Suzhou Nano Science and Technology. The TEM work was performed at the International Center for Dielectric Research (ICDR), Xi'an Jiaotong University, Xi'an, China. The authors also thank Mr. Ma and Ms. Lu for their help in using TEM.

#### References

- Q. Li, Y. He, J. Chang, L. Wang, H. Chen, Y. W. Tan, H. Wang and Z. Z. Shao, *J. Am. Chem. Soc.* 135, 14924 (2013).
- 2. O. S. Wolfbeis, Chem. Soc. Rev. 44, 4743 (2015).
- X. D. Wang, O. S. Wolfbeis and R. J. Meier, *Chem. Soc. Rev.* 42, 7834 (2013).
- 4. Z. Tang, N. A. Kotov and M. Giersig, *Science*, **297**, 237 (2002).
- 5. A. P. Alivisatos, Science, 271, 933 (1996).
- M. Bruchez, M. Moronne, P. Gin, S. Weiss and A. P. Alivisatos, *Science*, 281, 2013 (1998).
- X. L. Dai, Z. X. Zhang, Y. Z. Jin, Y. Niu, H. J. Cao, X. Y. Liang, L. W. Chen, J. P. Wang and X. G. Peng, *Nature*, 515, 96 (2014).
- X. Gao, Y. Cui, R. M. Levenson, L. W. Chung and S. Nie, *Nat. Biotechnol.* 22, 969 (2004).
- A. M. Derfus, W. C. Chan and S. N. Bhatia, Nano Lett. 4, 11 (2004).
- M. E. Åkerman, W. C. Chan, P. Laakkonen, S. N. Bhatia and E. Ruoslahti, *Proc. Natl. Acad. Sci.* 99, 12617 (2002).

- W. Liu, H. S. Choi, J. P. Zimmer, E. Tanaka, J. V. Frangioni and M. Bawendi, J. Am. Chem. Soc. 129, 14530 (2007).
- T. Jamieson, R. Bakhshi, D. Petrova, R. Pocock, M. Imani and A. M. Seifalian, *Biomaterials*, 28, 4717 (2007).
- 13. A. B. Djurišić and H. L. Yu, Small, 2, 944 (2006).
- J. Chen, D. Zhao, C. Li, F. Xu, W. Lei, L. Sun, A. Nathan and X. W. Sun, Sci. Rep. 4, 4085 (2014).
- H. M. Xiong, Y. Xu, Q. G. Ren and Y. Y. Xia, J. Am. Chem. Soc. 130, 7522 (2008).
- A. Fulati, S. M. Ali. Usman, M. Riaz, G. Amin,
   O. Nur and M. Willander, Sensors 9, 8911 (2009).
- J. Joo, S. G. Kwon, J. H. Yu and T. Hyeon, Adv. Mater. 17, 1873 (2005).
- F. Qu, D. R. Santos, N. O. Dantas, A. F. G. Monte and P. C. Morais, *Phys. E.* 23, 410 (2004).
- K. F. Lin, H. M. Cheng, H. C. Hsu, L. J. Lin and W. F. Hsieh, *Phys. Lett.* 409, 208 (2005).
- M. K. Patra, M. Manoth and V. K. Singh, *J. Lumin.* 129, 320 (2009).
- L. Spanhel and M. A. Anderson, J. Am. Chem. Soc. 113, 2826 (1991).
- 22. W. Z. Ostwald, Phys. Chem. 37, 385 (1901).
- M. Yue, J. Si, L. Yan, Y. Yu and X. Hou, Opt. Mater. Exp. 8, 698 (2018).
- 24. G. W. Yang, Prog. Mater. Sci. 52, 648 (2007).
- J. Xiao, P. Liu, C. X. Wang and G. W. Yang, *Prog. Mater. Sci.* 87, 140 (2017).
- J. Xiao, P. Liu and G. W. Yang, Nanoscale 7, 6114 (2015).
- 27. J. Xiao, P. Liu, L. Li and G. Yang, *J. Phys. Chem. C* **119**, 2239 (2015).
- H. Zeng, W. Cai, B. Cao, J. Hu, Y. Li and P. Liu, Appl. Phys. Lett. 88, 181905 (2006).
- H. Zeng, G. Duan, Y. Li, S. Yang, X. Xu and W. Cai, *Adv. Funct. Mater.* 20, 561 (2010).
- 30. V. Nguyen, L. Yan, J. Si and X. Hou, *J. Appl. Phys.* **117**, 084304 (2015).
- H. Xu, L. Yan, V. Nguyen, Y. Yu and Y. Xu, Appl. Surf. Sci. 414, 238 (2017).
- 32. S. Sudhagar, S. Sathya, K. Pandian and B. S. Lakshmi, *Biotechnol. Lett.* **33**, 1891 (2011).
- Y. S. Fu, X. W. Du, S. A. Kulinich, J. S. Qiu, W. J. Qin, R. Li, J. Sun and J. Liu, J. Am. Chem. Soc. 129, 16029 (2007).
- A. B. Moghaddam, T. Nazari, J. Badraghi and M. Kazemzad, Int. J. Electrochem. Sci. 4, 247 (2009).
- S. Bai, J. Hu, D. Li, R. Luo, A. Chen and C. C. Liu, J. Mater. Chem. 21, 12288 (2011).
- H. Zeng, Z. Li, W. Cai, B. Cao, P. Liu and S. Yang,
   J. Phys. Chem. B 111, 14311 (2007).
- V. Nguyen, L. Yan, H. Xu and M. Yue, Appl. Surf. Sci. 427, 1118 (2018).

- 38. R. S. Ajimsha, G. Anoop, A. Aravind and M. K. Jayaraj, *Solid-State Lett.* **11**, K14 (2008).
- K. Vanheusden, W. L. Warren, C. H. Seager, D. R. Tallant, J. A. Voigt and B. E. Gnade, *J. Appl. Phys.* 79, 7983 (1996).
- D. C. Look, G. C. Farlow, P. Reunchan, S. Limpijumnong, S. B. Zhang and K. Nordlund, Rev. Lett. 95, 225502 (2005).
- 41. B. Stuart, Infrared Spectroscopy: Fundamentals and Applications, 1st edn. (John Wiley, Sons, Ltd, 2004), pp. 80–81.
- Y. R. Luo, Handbook of Bond Dissociation Energies in Organic Compounds, 1st edn. (CRC Press, Boca Raton, Florida, 2002), pp. 213–268.
- 43. J. L. Mergny and J. Laurent, *Oligonucleotides* 13, 515 (2003).
- 44. J. M. Sanchez-Ruiz, Biophys. Chem. 148, 1 (2010).
- 45. C. H. Hsia, A. Wuttig and H. Yang, *ACS Nano.* **5**, 9511 (2011).
- R. Samy, T. Glawdel and C. L. Ren, Anal. Chem. 80, 369 (2008).

- 47. C. Gota, K. Okabe, T. Funatsu, Y. Harada and S. Uchiyama, *J. Am. Chem. Soc.* **131**, 2766 (2009).
- 48. D. Valerini, A. Creti, M. Lomascolo, L. Manna, R. Cingolani and M. Anni, *Phys. Rev. B.* **71**, 235409 (2005).
- X. Wen, J. A. Davis, L. Van Dao, P. Hannaford,
   V. A. Coleman, H. H. Tan, C. Jagadish, K. Koike,
   S. Sasa and M. Inoue, Appl. Phys. Lett. 90, 221914 (2007).
- X. Wen, A. Sitt, P. Yu, Y. R. Toh and J. Tang, Phys. Chem. Chem. Phys. 14, 3505 (2012).
- P. Yu, X. Wen, Y. R. Toh and J. Tang, J. Phys. Chem. C 116, 25552 (2012).
- E. J. McLaurin, R. B. Liam and R. G. Daniel, *Chem. Mater.* 25, 1283 (2013).
- Y. Cui, R. Song, J. Yu, M. Liu, Z. Wang and C. Wu, *Adv. Mater.* 27, 1420 (2015).
- A. E. Albers, E. M. Chan, P. M. McBride, C. M. Ajo-Franklin, B. E. Cohen and B. A. Helms, *J. Am. Chem. Soc.* 134, 9565 (2012).